Ruthenium based photosensitizer/catalyst supramolecular architectures in light driven water oxidation

Max Burian [a], Zois Syrgiannis [b,c], Giuseppina La Ganga [d], Fausto Puntoriero [d], Mirco Natali [e], Franco Scandola [e], Sebastiano Campagna [d,*], Maurizio Prato [c,f,g], Marcella Bonchio [b], Heinz Amenitsch [a,*], Andrea Sartorel [b,*]

[a] Institute of Inorganic Chemistry, Graz University of Technology, Stremayrgasse 9/IV, Graz 8010, Austria
[b] Department of Chemical Sciences, University of Padova and Institute on Membrane Technology, Unit of Padova, via F. Marzolo 1, 35131 Padova, Italy
[c] Department of Pharmaceutical Sciences, University of Trieste, via L. Giorgieri 1, 34127 Trieste, Italy
[d] Department of Chemical, Biological, Pharmaceutical and Environmental Sciences, University of Messina and Centro Interuniversitario per la Conversione Chimica dell'Energia Solare, Section of Messina, Via Sperone 31, 98166 Messina, Italy
[e] Department of Chemical and Pharmaceutical Sciences, University of Ferrara, via Fossato di Mortara 17-19, 44121 Ferrara, Italy
[f] Carbon Nanobiotechnology Laboratory, CIC biomaGUNE, Paseo de Miramón 182, 20009 Donostia-San Sebastian, Spain
[g] Basque Fdn Sci, Ikerbasque, Bilbao 48013, Spain

ARTICLE INFO

Article history:
Received 17 February 2016
Received in revised form 4 April 2016
Accepted 5 April 2016
Available online 22 April 2016

Keywords:
Water oxidation
Ruthenium polypyridine photosensitizers
Ruthenium polyoxometalate
Small-Angle X-ray Scattering

ABSTRACT

Light driven water oxidation is a key step in artificial photosynthesis, aimed at splitting water into hydrogen and oxygen with sunlight. In such process, the interactions between a photosensitizer (PS) and a water oxidation catalyst (WOC) play a crucial role in the rates of photoinduced electron transfers, determining the overall quantum efficiency of the system. In this work, by means of Small Angle X-ray Scattering (SAXS) we investigate the nature of the aggregates between ruthenium polypyridine photosensitizers (Rubpy and Ru_4dend) and a tetraruthenium polyoxometalate (Ru_4POM) water oxidation catalyst. Aggregate scattering is confirmed by the strong intensity-increase in the low-*q* regime, whereas the power law-fit of this region show slopes between −3 and −4, suggesting globular and porous aggregates. Intermolecular PS/WOC distances lower than 3 nm support the observed fast photoinduced electron transfers (<120 ps), however the proximity of the two components in the hybrids is also responsible for fast charge recombination. Approaches for inhibiting such undesired process are discussed.

1. Introduction

Artificial photosynthesis yearns for splitting water into hydrogen and oxygen exploiting sunlight (Eq. (1)), and appears as a promising route towards the development of renewable and inexhaustible fuels [1]:

$$2H_2O + \text{sunlight} \rightarrow 2H_2 + O_2 \quad (1)$$

The design and development of photosynthetic devices [2] may take inspiration from the natural process, that foresees a suitable architecture of functional modules. In synergy, the final framework needs to be capable of light absorption, energy and electron transfer, charge separation, and catalytic routines where hydrogen and oxygen are concomitantly generated [3]. In order to overcome the complexity of such assemblies as well as the challenges of interfacing all different functionalities, optimization of the involved components is often carried on separately [4].

In particular, light driven water oxidation, which has often been considered as the bottleneck of the entire process, takes advantage of a three components sacrificial system, composed by a water oxidation catalyst (WOC), a photosensitizer (PS), and a primary, sacrificial electron acceptor (SA), Scheme 1. Upon light absorption by the photosensitizer and generation of its excited state, an electron flow WOC→PS→SA is induced [5]; when this step is efficiently replicated several times, it ultimately leads to the formation of an oxidized form of the WOC, capable of oxidizing water to oxygen [6]. Typically, the persulfate dianion $S_2O_8^{2-}$ is employed as the SA, in virtue of its irreversible decomposition upon electron acceptance, which avoids unproductive, charge recombination events [5]. Concerning the photosensitizer PS, ruthenium polypyridine complexes have been widely considered due to their extended absorbance in the visible region, a suitable lifetime of the triplet

* Corresponding authors.

http://dx.doi.org/10.1016/j.ica.2016.04.010

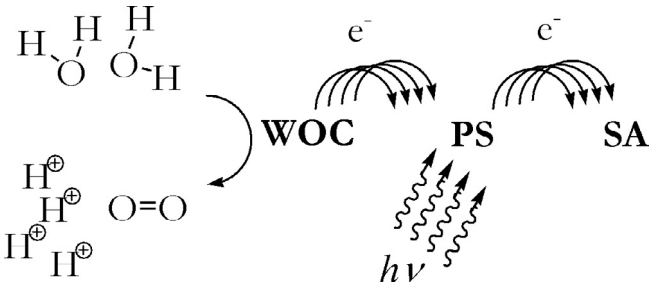

Scheme 1. Schematic representation of a three components system for light driven water oxidation, composed by a water oxidation catalyst (WOC), a photosensitizer (PS) and a sacrificial electron acceptor (SA).

manifold excited state as well as the high redox potential to feed the water oxidation process [5].

The forerunner of such coordination complexes is tris(2,2′-bipyridine)ruthenium(II), hereafter Rubpy (Fig. 1) [5,7], while the use of ruthenium based dendrimeric derivatives, such as $[Ru\{(\mu\text{-dpp})Ru(bpy)_2\}_3]^{8+}$ (dpp = 2,3-bis(2′-pyridyl)pyrazine), hereafter Ru_4dend (Fig. 1) [7–9], has provided significant advantages in terms of extended absorption in the visible spectra of solar light emission [9]. In particular, Rubpy and Ru_4dend photosensitizers have been combined with a tetraruthenium polyoxometalate $\{Ru_4(\mu\text{-}O)_4(\mu\text{-}OH)_2(H_2O)_4[\gamma\text{-}SiW_{10}O_{36}]\}^{10-}$ (hereafter Ru_4POM,

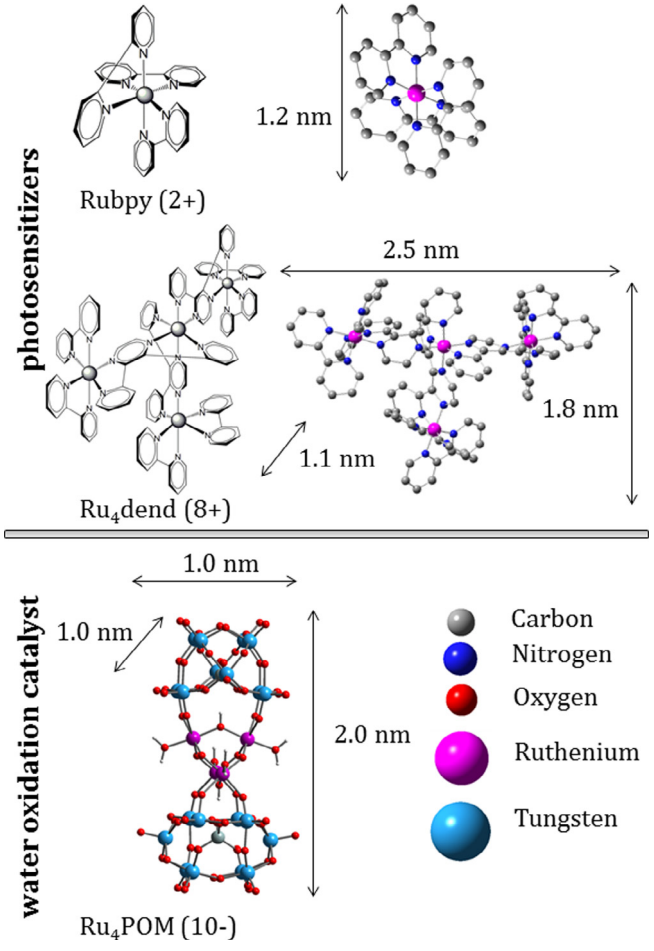

Fig. 1. Ruthenium polypyridine photosensitizers and tetraruthenium polyoxometalate water oxidation catalyst employed in this work. Some key dimensions of the three molecules are provided.

Fig. 1) as the water oxidation catalyst, reaching notable efficiency and unprecedented quantum yield towards oxygen generation, using persulfate as the sacrificial electron acceptor [10–12]. In both cases, the occurrence of supramolecular PS/WOC aggregates, formed by electrostatic based ion pairs between the cationic photosensitizers and the polyanionic WOC had a remarkable impact in the overall efficiency of the light activated cycle [11,12]. In particular, Ru_4dend/Ru_4POM aggregation in 1:1 stoichiometry, is responsible for fast, reductive quenching of Ru_4dend triplet excited state by Ru_4POM, occurring in a hundred ps timescale [12b], and initiating the cascade of electron transfer events that ultimately lead to O_2 production with a quantum yield of 0.30 [12].

In this work, we investigate the structural features of these electrostatic aggregates by means of Small Angle X-ray Scattering (SAXS), which is recognized as a state-of-the-art characterization technique for nano-assembly in solution [13]. From a single measurement this technique allows to gain insights on a wide structural range, starting from an estimate on the aggregates' size and morphology down to mean intermolecular distances within the assembly. The combination of SAXS evidence with Transmission Electron Microscopy (TEM) imaging, and elemental mapping techniques, has a definite potential regarding the characterization of competent photosynthetic nano-systems, formed in water by the supramolecular PS/WOC assembly. The final aim is to build effective structure–reactivity descriptors for the design of functional materials and photoelectrodes.

2. Experimental

2.1. Materials

Rubpy was purchased from Sigma–Aldrich as the dichloride, hexahydrate salt. Ru_4dend and Ru_4POM were synthesized according to the literature procedures [8c,14] and isolated as the PF_6^- and Na^+ salts, respectively.

2.2. Sample preparation

The Ru_4POM·Ru_4dend and Ru_4POM·Rubpy hybrid aggregates were obtained by simple mixing of precursors using ratios stated further below, by mixing stock solutions in 50/50 H_2O/tetrahydrofuran (THF) of Ru_4POM (1×10^{-4} M) and of Ru_4dend (1×10^{-4} M) or Rubpy (4×10^{-4} M). The actual mixing was performed ca 10 min before measurement. The mixed H_2O/THF was employed as the solvent due to a better dispersion of the aggregates with respect to pure aqueous media.

2.3. Small Angle X-ray Scattering (SAXS)

Small Angle X-ray Scattering experiments were performed at the Austrian SAXS beamline of Elettra synchrotron (Trieste, Italy) using 8 keV photon energy. The liquid samples were filled in standard 1.5 mm quartz capillaries whereas 6–8 consecutive images were taken over time, to rule out possible radiation damage by comparison of the scattering pattern. A two-dimensional image-plate detector (Mar300, Germany) was placed at a distance of approximately 90 cm to obtain an accessible q-range from 0.15 to 9.25 nm^{-1}. A reference measurement was made using silver-behenate as a standard for the calibration of the angular regime. Azimuthal integration of the 2D images was done using the Fit2D program [15]. The resulting integrated scattering curves were corrected for dark-current, normalized by sample transmission and subsequently the background was subtracted using the pure solvent-scattering.

2.4. Transmission Electron Microscopy (TEM)

TEM images were acquired using a Philips EM 208 microscope, with accelerating voltage of 100 kV. Samples were prepared by drop casting of the mixed samples onto a carbon coated 200 mesh Ni grid (EM Sciences, Gibbstown, NJ) followed by solvent evaporation under vacuum.

2.5. Dynamic light scattering (DLS)

DLS experiments were performed with a Malvern Zetasizer Nano-S instrument, equipped with a quartz cuvette thermostated at 25 °C; laser wavelength 633 nm.

3. Results and discussion

3.1. SAXS

Synchrotron SAXS measurements were conducted on $Ru_4POM{\cdot}Ru_4dend$ hybrid aggregates, prepared by mixing an equimolar amount of Ru_4dend and Ru_4POM precursors, as well as a comparative measurement of a 1:4 Ru_4POM:Rubpy mixture (association of Ru_4POM with Ru_4dend and Rubpy in 1:1 and 1:4 ratios, respectively, was observed by means of conductometric titrations [11a,12b], and can be justified on the basis of the charge-balance provided by the cationic photosensitizer with respect to the Ru_4POM polyanion, see Fig. 1). The scattering from both systems are shown in Fig. 2; the first clear observation is the strong intensity-increase in the low-q regime, which is characteristic for aggregate-scattering, as it is evident also from TEM images of the same mixtures as seen in Fig. 3.[1] The slopes of the Porod fits in the low-q regime of −2.98 ($Ru_4POM{\cdot}Ru_4dend$) and −4.02 ($Ru_4POM{\cdot}Rubpy$), suggest the presence of globular aggregates, that appear to be more porous in the case of $Ru_4POM{\cdot}Ru_4dend$ compared to $Ru_4POM{\cdot}Rubpy$, as indicated by the lower absolute value of the slope [16]. An explanation for the increased porosity might be the higher size of Ru_4dend with respect to Rubpy (see Fig. 1): the ruthenium dendrimer acts as a "spacer" between interacting molecules, whereas in the case of the quasi-spherical and significantly smaller Rubpy, a more compact packing can be envisioned.

More interestingly, both curves exhibit rather broad correlation peaks in the mid to high-q regime, that correspond to intermolecular distances in the aggregate (indeed, these peaks are not observed in the isolated solution of Ru_4POM, Ru_4dend, or Rubpy). To better understand these features, one should keep in mind that the recorded intensity in an X-ray scattering experiment is proportional to the square of the electron density difference in the sample. In the present case, the SAXS patterns will be then dominated by scattering from the heavy atoms (W atoms from the polyoxotungstate cage of Ru_4POM), which, as a side effect, makes the polypyridine groups comparably transparent to the X-rays. Therefore the observed correlation peaks most likely represent mean distances between Ru_4POM molecules inside the aggregates (see Table 1). In particular, the broad nature of the peaks immediately implies that the molecular arrangements are disordered in the sense that no coherent long range order exists, hence the terminology *mean* intermolecular-distance is used herein. It is, however, intriguing that the positions of the correlation peaks **A**, **B** and **C** fall in a similar region, for both $Ru_4POM{\cdot}Ru_4dend$ and the $Ru_4POM{\cdot}Rubpy$ nano-hybrids (Fig. 2),

[1] The presence of large aggregates is detected also with dynamic light scattering (DLS) experiments, although the low quality of the fitting of the correlation function, likely ascribable to non-monodisperse particles, does not allow a precise estimation of the size (see Fig. S3).

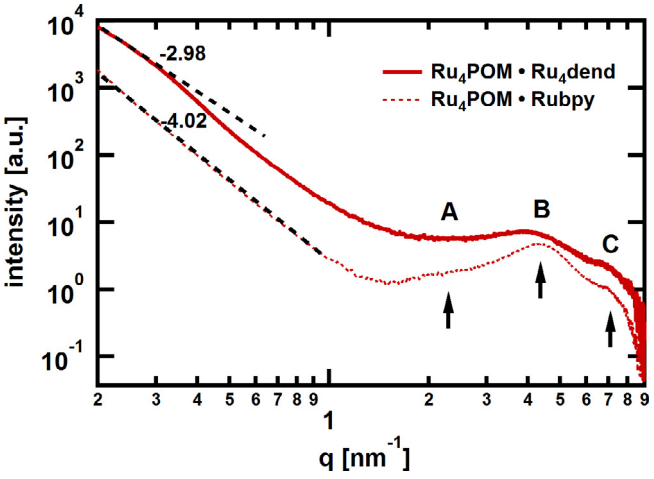

Fig. 2. SAXS data recorded for both $Ru_4POM{\cdot}Ru_4dend$ (1:1 ratio) and $Ru_4POM{\cdot}Rubpy$ (1:4 ratio) in H_2O/THF solution. The black-dotted lines represent the Porod fits in the low-q regime that reveal a more porous structure in the case of $Ru_4POM{\cdot}Ru_4dend$. The black arrows indicate the correlation peaks (**A**, **B**, **C**) resulting from inter-molecular mean distances (see Fig. S1), whereas the exact d-spacings of the reflections are found in Table 1. Error-bars are omitted for clarity.

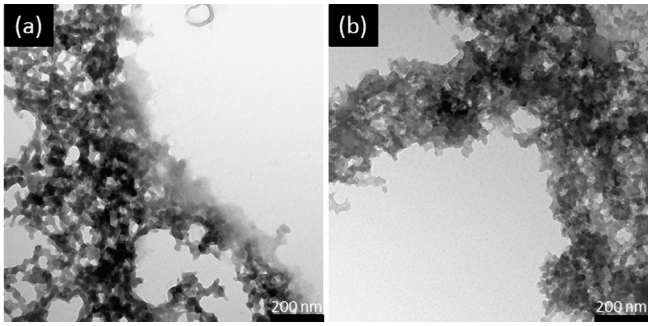

Fig. 3. TEM images of the aggregates (a) $Ru_4POM{\cdot}Ru_4dend$ and (b) $Ru_4POM{\cdot}Rubpy$. Scale bar: 200 nm.

implying the occurrence of analogous structural motifs within both aggregates. A closer look at the d-spacing values in Table 1 shows that both **A** and **B** peaks are found at higher values in the case of $Ru_4POM{\cdot}Ru_4dend$, thus supporting the notion that the bulky tetraruthenium dendrimer increases the mean distance between the Ru_4POM scattering centres.

To further investigate the nature of the correlation peaks and of the corresponding structural parameter (mean Ru_4POM distance) as a function of the $Ru_4POM{\cdot}Ru_4dend$ stoichiometry SAXS measurements were repeated at Ru_4POM:Ru_4dend = 0.5:1 ratio. In these conditions, due to strong electrostatic association, ca. 50% of the Ru_4dend is present in solution and the overall amount of $Ru_4POM{\cdot}Ru_4dend$ aggregates is halved, while their composition and nano-morphology are expected to be unchanged [12b]. Indeed, as seen in Fig. 4 (full scattering curves can be found in the Supporting information), the low-q aggregate scattering is very similar for both mixing ratios (Porod slope of −3.03 for Ru_4POM:Ru_4dend = 0.5:1), which implies that the nano-morphology of the aggregates is unchanged. This was further confirmed by comparable **A**, **B** and **C** d-spacings values (Table 1). In regard of the previously determined correlation peaks, two different behaviors can be observed as far as peak intensities are concerned: while peaks **A** and **B** decrease comparable to the low-q regime, peak **C** is only slightly lowered. To put these observations into context, it should be noted that the measured scattering intensity in such a X-ray scattering experiment

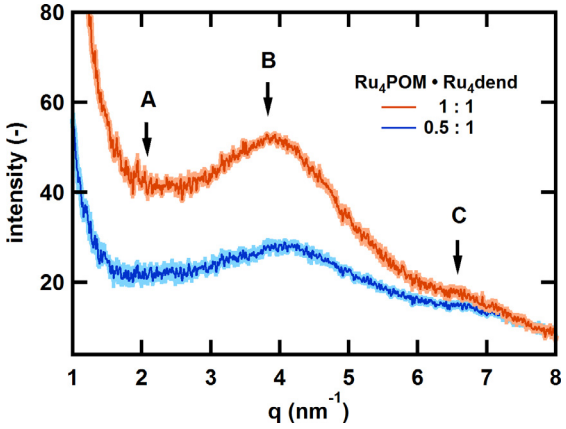

Fig. 4. SAXS data of Ru_4POM:Ru_4dend samples mixed 1:1 and 0.5:1 in H_2O/THF solution. The previously determined correlation peaks are marked by black arrows. For better comparability, the curves were normalized to the Ru_4dend concentration in the final mixture. Error bars are represented by the light color background of the curves. As this data suggests, with decreasing Ru_4POM concentration, peaks A and B are significantly decreased, while peak C appears to be invariant. (For interpretation of the references to colour in this figure legend, the reader is referred to the web version of this article.)

Table 1
Mean intermolecular *d*-spacings obtained from the correlation peaks as marked by the black arrows in Fig. 2.

	A (nm)	**B** (nm)	**C** (nm)
Ru_4POM·Ru_4dend	3.06 (0.20)	1.64 (0.09)	0.95 (0.10)
Ru_4POM·Rubpy	2.56 (0.48)	1.47 (0.03)	0.97 (0.06)
Ru_4POM·Ru_4dend (0.5:1)	2.89 (0.27)	1.57 (0.10)	0.91 (0.12)

Errors are given in brackets. The corresponding fits can be found in Fig. S1 in the Supporting information.

directly correlates with the concentration of the aggregates, assuming all other parameters remain constant [16]. In this case, since the nano-morphology of the aggregates is identical, a reduction of the relative Ru_4POM concentration should hence scale down corresponding scattering features by the same amount. The data in Fig. 4 clearly show that this predicted behavior can actually be identified in the case of peaks **A** and **B**. On the other hand, the rather unexpected non-linear behavior of peak **C** cannot as easily be connected to one of the nano-aggregate. An indisputable attribution of peak **C** will be therefore subject to further investigation.[2]

3.2. Intermolecular arrangement

The obvious subsequent step towards elucidating the intermolecular features seen in the SAXS data is a comparison of the retrieved mean distances with dimensions from previously established theoretical models. Ru_4POM has already been structurally characterized and described in literature [14]. An analogous characterization is missing for Ru_4dend, mostly due to the existence of geometrical and stereo-isomers [8,17]; however the approximate dimensions of this latter species can be estimated, as shown in Fig. 1. Before focusing on the information above about mean distances gained directly from the scattering data, an important consideration should be kept in mind: as seen by the −3 slope in the low-*q* regime of the SAXS measurements, the Ru_4POM·Ru_4dend aggregate morphology appears to be rather random and globular, implying that no preferred growth direction exists (slope values of −1 and −2 are instead expected for 1-D and 2-D aggregates, respectively) [16]. This also means that there is no molecular alignment or orientation relation since this would have anisotropic consequences on the underlying growth mechanism and therefore on the aggregate shape. All of the above observations together with the broad nature of the peaks are a clear indication that no long range order between the molecules exists. Accordingly, the observed correlation peaks in the scattering data have to be the result from a three-dimensionally disordered system, representing the spherically-averaged mean distance between the molecular components.

With this in mind the previous observations can now be put in a more global context. The molecular structure of Ru_4POM represent a fairly rigid building block, where the atomic distances are well known from the solid-state crystallographic analysis. As a first SAXS model a double ellipsoid arrangement was postulated [18], which can be simplified as a cylindrical geometry with 1 nm of diameter and 2 nm in height. A comparison of these dimensions with the measured mean distances in the aggregate of 1.64 and 3.06 nm shows that their assignment to a Ru_4POM–Ru_4POM mean distance is plausible when assuming intercalation of Ru_4dend molecules with different geometrical conformations.

3.3. Implication of Ru_4POM·Ru_4dend assembly on photoinduced electron transfer

The electrostatic association between Ru_4POM and Ru_4dend and the intimate distance between the two components in the aggregate (considering intercalation of one Ru_4dend between two Ru_4POM molecules, an estimate of the Ru_4POM–Ru_4dend distance is given by half values of the observed *d*-spacings, and therefore be in the 0.8–1.5 nm range) fully support the fast photoinduced, electron transfer leading to reductive quenching of the triplet metal-to-ligand charge-transfer (MLCT) excited state of Ru_4dend by Ru_4POM. Such a process is characterized by a relatively high driving force of $\Delta G = -0.58$ eV and takes place with a time constant of about 126 ps in phosphate buffer at pH 7 [12b,19]. Charge recombination is estimated to be even faster, as demonstrated by the non-accumulation of the charge-separated state in the ultrafast pump–probe spectroscopic experiments, and agrees with an even larger driving force (close to −1.1 eV) [12b]. This suggests that both forward and back electron transfer processes in the associated Ru_4POM·Ru_4dend systems are not slowed down by the nuclear barrier effects usually occurring in restricted environments as a consequence of significant increase in reorganization energy [20]. Such result can be attributed to the "porous" nature of the Ru_4POM·Ru_4dend system discussed above, that would let enough mobility to the donor–acceptor pair to overcome problems due to the expected reorganization energy.

4. Conclusion

In this work we have investigated by means of Small Angle X-ray Scattering the nature of aggregates between ruthenium polypyridine photosensitizers Ru_4dend and Rubpy, and a tetraruthenium water oxidation catalyst Ru_4POM, that provide very efficient systems in light driven water oxidation with persulfate as electron acceptor [10–12]. Power law-fit in the low-*q* regime between −3 and −4 are diagnostic for globular, porous aggregates, that grow in a three dimensional, disordered network. Intermolecular PS/WOC distances lower than 3 nm are compatible with fast

[2] The seemingly constant scattering behavior of peak **C** under changing Ru_4POM concentrations is unusual. While the present data doesn't allow a decisive assignment to a specific molecular arrangement, it might help to exclude possible conformations. The comparison of the corresponding mean molecular distance of 0.97 nm (retrieved from the peak position) with the structural dimensions of Ru_4POM (see Fig. 1), together with the unaffected scattering intensity under changing conditions, makes an attribution of **C** to a Ru_4POM–Ru_4POM distance improbable.

photoinduced electron transfers observed in a hundred of ps timescale [12b]; however the proximity of the two components in the aggregates promotes also very fast back electron transfer, that could be detrimental for the overall efficiency of the PS/WOC assembly when embedded onto a regenerative photoelectrode. This justifies the present, extensive efforts in the development of redox relays [21], aimed at decreasing charge recombination rates in photoactive assemblies. Moreover, parameters such as pore size and active surface area of the aggregates should be considered, since they could impact the overall photocatalytic performance of the device.

Acknowledgments

Financial support from the Italian Ministero dell'Università e della Ricerca (MIUR), (FIRB RBAP11C58Y, "NanoSolar" and PRIN 2010 "Hi-Phuture") and COST actions CM1205 "CARISMA: CAtalytic RoutInes for Small Molecule Activation" and CM1202 "PERSPECT-H2O" are gratefully acknowledged.

Appendix A. Supplementary material

Supplementary data associated with this article can be found, in the online version, at http://dx.doi.org/10.1016/j.ica.2016.04.010.

References

[1] (a) S. Berardi, S. Drouet, L. Francàs, C. Gimbert-Suriñach, M. Guttentag, C. Richmond, T. Stoll, A. Llobet, Chem. Soc. Rev. 43 (2014) 7501;
(b) K.S. Joya, Y.F. Joya, K. Ocakoglu, R. van de Krol, Angew. Chem., Int. Ed. 52 (2013) 10426;
(c) I. Yasuo, Coord. Chem. Rev. 257 (2013) 171.
[2] J.R. McKone, N.S. Lewis, H.B. Gray, Chem. Mater. 26 (2014) 407.
[3] N. Armaroli, V. Balzani, Angew. Chem., Int. Ed. 46 (2007) 52.
[4] J.H. Alstrum-Acevedo, M.K. Brennaman, T.J. Meyer, Inorg. Chem. 44 (2005) 6802.
[5] (a) A. Sartorel, M. Bonchio, S. Campagna, F. Scandola, Chem. Soc. Rev. 42 (2013) 2262;
(b) F. Puntoriero, A. Sartorel, M. Orlandi, G. La Ganga, S. Serroni, M. Bonchio, F. Scandola, S. Campagna, Coord. Chem. Rev. 255 (2011) 2594.
[6] S. Piccinin, A. Sartorel, G. Aquilanti, A. Goldoni, M. Bonchio, S. Fabris, Proc. Acad. Natl. Sci. U.S.A. 110 (2013) 4917.
[7] (a) S. Serroni, S. Campagna, F. Puntoriero, C. Di Pietro, N.D. McClenaghan, F. Loiseau, Chem. Soc. Rev. 30 (2001) 367;
(b) V. Balzani, A. Juris, Coord. Chem. Rev. 211 (2001) 97;
(c) V. Balzani, P. Ceroni, A. Juris, M. Venturi, S. Campagna, F. Puntoriero, S. Serroni, Coord. Chem. Rev. 219–221 (2001) 545;
(d) F. Puntoriero, F. Nastasi, M. Cavazzini, S. Quici, S. Campagna, Coord. Chem. Rev. 251 (2007) 536.
[8] (a) W.R. Murphy, K.J. Brewer, G. Gettliffe, J.D. Petersen, Inorg. Chem. 28 (1989) 81;
(b) S. Campagna, G. Denti, L. Sabatino, S. Serroni, M. Ciano, V. Balzani, J. Chem. Soc., Chem. Commun. (1989) 1500;
(c) G. Denti, S. Campagna, L. Sabatino, S. Serroni, M. Ciano, V. Balzani, Inorg. Chem. 29 (1990) 4750.
[9] G. La Ganga, F. Nastasi, S. Campagna, F. Puntoriero, Dalton Trans. (2009) 9997.
[10] Y.V. Geletii, Z. Huang, Y. Hou, D.G. Musaev, T. Lan, C.L. Hill, J. Am. Chem. Soc. 131 (2009) 7522.
[11] (a) M. Natali, M. Orlandi, S. Berardi, S. Campagna, M. Bonchio, A. Sartorel, F. Scandola, Inorg. Chem. 51 (2012) 7324;
(b) M. Orlandi, R. Argazzi, A. Sartorel, M. Carraro, G. Scorrano, M. Bonchio, F. Scandola, Chem. Commun. 46 (2010) 3152.
[12] (a) F. Puntoriero, G. La Ganga, A. Sartorel, M. Carraro, G. Scorrano, M. Bonchio, S. Campagna, Chem. Commun. 46 (2010) 4725;
(b) M. Natali, F. Puntoriero, C. Chiorboli, G. La Ganga, A. Sartorel, M. Bonchio, S. Campagna, F. Scandola, J. Phys. Chem. C 119 (2015) 2371.
[13] (a) C.D. Putnam, M. Hammel, G.L. Hura, J.A. Tainer, Q. Rev. Biophys. 40 (2007) 191;
(b) A.S. Weingarten, R. Kazantsev, L.C. Palmer, M. McClendon, A.R. Koltonow, A. P.S. Samuel, D.J. Kiebala, M.R. Wasielewski, S.I. Stupp, Nat. Chem. 6 (2014) 964;
(c) M.R. Wasielewski, Acc. Chem. Res. 42 (2009) 1910;
(d) B. Marmiroli, H. Amenitsch, Eur. Biophys. J. Biophys. Lett. 41 (2012) 851.
[14] A. Sartorel, M. Carraro, G. Scorrano, R. De Zorzi, S. Geremia, N.D. McDaniel, S. Bernhard, M. Bonchio, J. Am. Chem. Soc. 130 (2008) 5006.
[15] A.P. Hammersley, S.O. Svensson, M. Hanfland, A.N. Fitch, D. Hausermann, High Pressure Res. 14 (4–6) (1996) 235.
[16] O. Glatter, O. Kratky, Small Angle X-ray Scattering, Academic Press, London, 1982.
[17] (a) G. Denti, S. Campagna, S. Serroni, M. Ciano, V. Balzani, J. Am. Chem. Soc. 114 (1992) 2944;
(b) S. Campagna, G. Denti, S. Serroni, A. Juris, M. Venturi, V. Ricevuto, V. Balzani, Chem. Eur. J. 1 (1995) 211.
[18] F.M. Toma, A. Sartorel, M. Iurlo, M. Carraro, P. Parisse, C. Maccato, S. Rapino, B. Rodriguez Gonzalez, H. Amenitsch, T. Da Ros, L. Casalis, A. Goldoni, M. Marcaccio, G. Scorrano, G. Scoles, F. Paolucci, M. Prato, M. Bonchio, Nat. Chem. 2 (2010) 826.
[19] Timescales in the order of ps are observed also for photoinduced electron transfers in covalently linked catalyst/sensitizer systems, see A. Montellano López, M. Natali, E. Pizzolato, C. Chiorboli, M. Bonchio, A. Sartorel, F. Scandola, Phys. Chem. Chem. Phys. 16 (2014) 12000.
[20] (a) G.L. Gaines, M.P. O'Neil, W.A. Svec, M.P. Niemczyk, M.R. Wasielewski, J. Am. Chem. Soc. 113 (1991) 719;
(b) P.Y. Chen, T.J. Meyer, Chem. Rev. 98 (1998) 1439. In such studies, a destabilization of the charge separated state of about 0.6 eV on passing from room temperature fluid solution to 77 rigid matrix (where the matrix can be viewed as a restricted environment) is calculated. The destabilization of the charge separated state there justifies the inefficiency of electron transfer with mild driving forces. Similar effects can occur as a function of increased nuclear barrier to the electron transfer.
[21] J.D. Megiatto Jr., D.D. Méndez-Hernández, M.E. Tejeda-Ferrari, A.-L. Teillout, M. J. Llansola-Portolés, G. Kodis, O.G. Poluektov, T. Rajh, V. Mujica, T.L. Groy, D. Gust, T.A. Moore, A.L. Moore, Nat. Chem. 6 (2014) 423.